Exploration of Novel Mono Hydroxamic Acid Derivatives as Inhibitors for Histone Deacetylase Like Protein (HDLP) by Molecular Dynamics Studies

Gunasingham Parthiban[1], Ramachandran Dushanan[2], Samantha Weerasinghe[3], Dhammike Dissanayake[3], and Rajendram Senthilnithy[2*]

[1]*Department of Chemistry, Eastern University, Vantharumoolai 30376, Sri Lanka*

[2]*Department of Chemistry, The Open University of Sri Lanka, Nugegoda 10250, Sri Lanka*

[3]*Department of Chemistry, University of Colombo, Colombo 00300, Sri Lanka*

Corresponding author:

email: rsent@ou.ac.lk

Received: April 18, 2022
Accepted: July 7, 2022

DOI: 10.22146/ijc.74167

Abstract: *The acetylation modification process of histone has an essential role in the epigenetic regulation of gene expression. This process is controlled by the balance between histone deacetylases (HDAC) and histone acetyltransferases (HAT). HDACs are thought to be vital for cell function. Particularly, higher HDAC expression is frequent in various cancers, resulting in the dysregulation of several target genes involved in cell proliferation, differentiation, and survival. In this study, the inhibitory feasibility of several HDAC inhibitors was investigated, including vorinostat (SAHA),* N*-hydroxy-3-phenylprop-2-enamide (CPD1),* N*-hydroxy-3-(pyridine-4-yl)prop-2-enamide (CPD2),* N*-hydroxy-3-(pyridine-2-yl)prop-2-enamide (CPD3), 4-(diphenylamino)-*N*-(5-(hydroxyamino)-5-oxopentyl)benzamide (CPD4), 2-(6-(((6-fluoronaphthalen-2-yl)methyl)amino)-3-azabicyclo[3.1.0]hex-3-yl)-*N*-hydroxypirimidine-5-carboxamide (CPD5), and* N*-(3-aminopropyl)-*N*-hydroxy-2-((naphthalene-1-yloxy)methyl)oct-2-enediamide (CPD6). By examining the stability of the enzyme, positional stability of the individual amino acids, and binding energies of HDLP-inhibitor complexes, the inhibitory feasibility was assessed. The complexes of the HDLP enzyme with SAHA, CPD4, CPD5, and CPD6 had higher stability than the other studied complexes, according to the results of trajectory analysis and the Ramachandran plot. Based on the calculated MM-PBSA binding free energies, the stability of the HDLP enzyme followed this order CPD4 > CPD5 > SAHA > CPD6 > CPD2 > CPD3 > CPD1. The drugability values followed the same trend as the previous ones. Based on the obtained* in silico *results, CPD4, CPD5, and CPD6 were discovered to be possible lead compounds as reference inhibitors of SAHA.*

Keywords: *epigenetic regulation; HDAC; MM-PBSA; Ramachandran plot; hydroxamic acid derivatives*

■ INTRODUCTION

Chemotherapy in cancer treatment has been a significant medical advance in past decades [1]. The medications utilized for chemotherapy have a limited therapeutic index, and the obtained results are only remedial and uncertain [2]. Even though specific biomacromolecules direct them, such techniques do not distinguish between cancerous and non-cancerous cells. Targeted therapy, in contrast, focuses on cancer-specific targets and signaling pathways [3]. Several studies have found that epigenetic pathways are essential in cancer development. Carcinogenesis is explained by genetic alterations and epigenetic processes (DNA methylation, histone modifications, and RNA deregulation) [4].

The electrostatic interactions of protein-DNA are influenced by the epigenetic control of gene expression functions through a series of post-translational chromatin modifications. These post-translational

modifications also produced docking sites for many chromatin-interacting proteins [5].

The acetylation of lysine residues found in the N terminal of core histone is one of the post-translational chromatin modifications that affect gene expression [6]. Acetylation and deacetylation of histones are restricted by the enzymes of histone acetyltransferase and histone deacetylase (HDACs) [7]. Alterations of gene expression are a hallmark of cancer, and evidence suggests an epigenetic mechanism mediates at fewest a component of these alterations [8]. Notably, the anomalous recruitment of HDACs has been mechanistically linked to different types of malignancies. One of the promising anticancer agents is HDAC inhibitors, and many natural and synthetic inhibitors get involved in clinical trials as possible antitumor agents [9].

Eighteen HDACs have been identified in humans and divided into four classes of two different protein families based on function and DNA sequence similarity. The proteins which belong to Class I (HDACs 1–3 and 8), Class II (HDACs 4–7, 9, and 10), and Class IV (HDAC 11) are a family of Zinc-dependent metalloproteins and Class III (SIRT 1–7) is the family of NAD^+ dependent proteins [10].

The basic information, such as the structure and dynamical properties of the inhibitor molecules and the HDAC enzyme complexes, may play a significant role in the HDAC inhibitor's selectivity and specificity [11]. The majority of HDAC inhibitors in and out of clinical trials inhibit all HDAC isoforms non-specifically, whereas 11 HDAC inhibitors act individually against some HDACs (HDAC isoform-selective inhibitors) or all types of HDACs (pan-inhibitors); however, the majority of HDAC inhibitors in and out of clinical trials inhibit all HDAC isoforms non-specifically [12]. SAHA is the canonical pan-inhibitor, regulating HDAC1 to HDAC9 activity with nearly similar potency [13]. The hydroxamic acid derivatives are more effective against tumors, according to recent studies. Therefore, this work included only hydroxamic acid derivatives. Hydroxamic acids have the general formula of RC(=O)N(R')OH [14-15].

Running a molecular dynamics (MD) simulation study covering all kinds of HDAC and inhibitors takes a while. Therefore, histone deacetylase-like protein (HDLP), which contains the majority of the amino acids in HDAC1 through HDAC9 and has a high degree of sequence similarity around the active region, was chosen for this computational experiment. The HDLP enzyme shares 80% sequence identity with HDAC8 (class I), making it very comparable to human class II HDACs in both sequence and function. The HDLP enzyme has a fold and an eight-stranded parallel -sheet in its topology, similar to deacetylase [16].

The link between the HDAC enzyme and inhibitors has been the subject of theoretical inquiry by numerous research teams. Research on the Rg, dynamical distance fluctuation between reactive centers on HDAC3 with CG1521, dihedral angle analysis of inhibitors, and RMSF research on the HDLP enzyme with the inhibitors valproic acid, TSA, and SAHA have all been reported [17]. Research has been done on the Zinc-SAHA binding mechanism [18-19]. However, there is disagreement on the role of hydrogen bonds, electrostatic interactions, and binding free energy in the interaction between HDAC inhibitors and HDAC enzymes in stabilizing the complex [17].

Because of this, drug development needs to compute binding affinities accurately for the protein-ligand system [20]. To anticipate the binding affinity of a protein and a ligand, several research teams employ various computer techniques. The best method for assessing the binding affinity of the protein-ligand complex is to estimate binding free energy using molecular dynamics simulations. Additionally, free energy calculations have been carried out utilizing Poisson-Boltzmann surface area (MM-PBSA), classical molecular mechanics, and molecular docking [21].

The in-silico method for determining the binding energy of the protein-inhibitor complex, the relative stability of protein-inhibitor contacts, the flexibility of the active site residues, quantitative structure-activity relationships, and inhibitor linker region analysis are the main topics of this study.

■ COMPUTATIONAL METHODS

The structure of Histone Deacetylase-like Protein (PDB ID 1ZZ1) (Fig. 1) was taken from the RCSB

database [16]. UCSF Chimera software was employed to prepare the protein, and the resulting enzyme structure was employed for molecular docking [22].

The used inhibitors were optimized at the quantum chemistry composite method CBS-QB3. The Complete Basis Set (CBS) approaches developed by Petersson and colleagues include the CBS-QB3. Gaussian G09 software was used for the geometry optimization process [23]. The CBS-APNO is the most accurate Complete Basis Set method; however, the computational effort is high, and CBS-4M has high errors compared to others. Therefore, the CBS-QB3 method is employed, and the error of CBS-QB3 is approximately about 1.1 kcal mol^{-1} errors. Using the Avogadro software, each optimized structure was converted to .pdb format [24]. The IUPAC names of such seven used inhibitors are listed in Table 1, and the structures are given in Fig. 2.

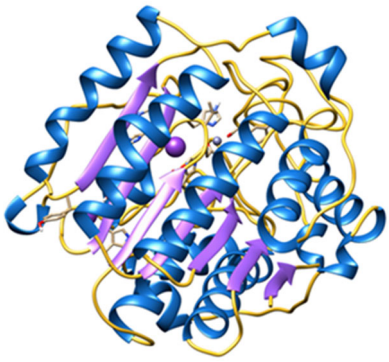

Fig 1. The 3D crystallographic structure of the HDLP enzyme with alpha-helices (blue), beta-sheets (violet), and loops (yellow)

Table 1. IUPAC names of the studied inhibitors

IUPAC name	Compound ID
N-hydroxy-*N'*-phenyloctanediamide	SAHA
N-hydroxy-3-phenylprop-2-enamide	CPD1
N-hydroxy-3-(pyridin-4-yl)prop-2-enamide	CPD2
N-hydroxy-3-(1H-pyrrol-2-yl)prop-2-enamide	CPD3
4-(diphenylamino)-*N*-(5-(hydroxyamino)-5-oxopentyl)benzamide	CPD4
2-(6-(((6-fluoronaphthalen-2-yl)methyl)amino)-3-azabicyclo[3.1.0]hex-3-yl)-*N*-hydroxypyrimidine-5-carboxamide	CPD5
N-(3-aminopropyl)-N-hydroxy-2-((naphthalen-1-yloxy)methyl)oct-2-enediamide	CPD6

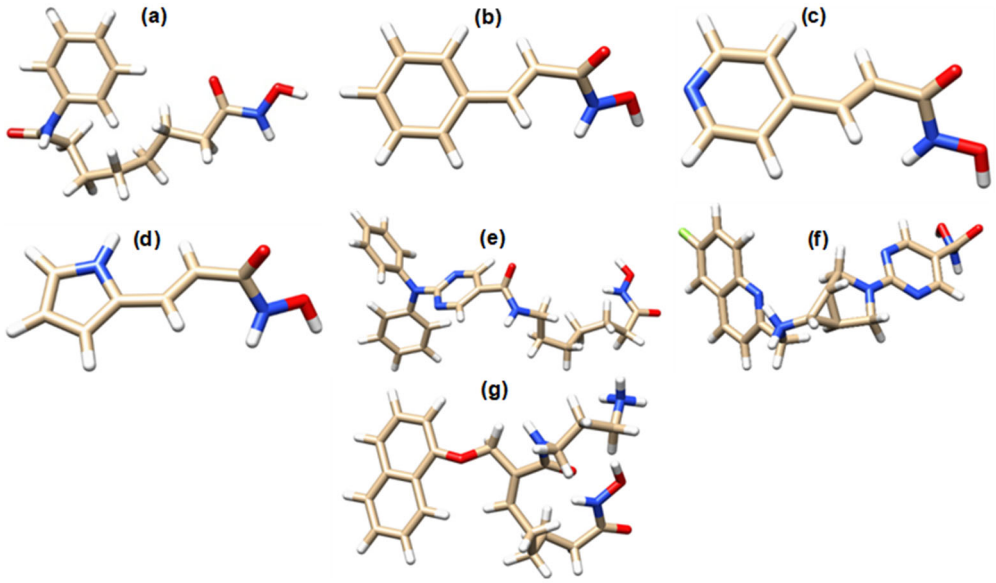

Fig 2. The employed structures of the HDAC inhibitors in this study. (a) SAHA, (b) CPD1, (c) CPD2, (d) CPD3, (e) CPD4, (f) CPD5, and (g) (CPD6) (The colors peach, red, white, and blue represent the atoms of carbon, oxygen, hydrogen, and nitrogen respectively). Each structure was optimized using Gaussian 09

Molecular Docking

The optimized inhibitor structure was docked to the HDLP enzyme using the AutoDock Tools 1.5.6 software [25]. The number of rotatable bonds in each inhibitor was changed to account for the flexibility of the inhibitor during the docking process [26]. Pymol was employed to combine the HDLP protein and inhibitors [27]. The best binding pose was selected based on the lowest binding score, and this pose was used as the starting configuration for the molecular dynamics simulations [28].

Molecular Dynamics Simulation

The software GROMACS 4.5.6 was used to run the molecular dynamics simulation [29]. For the HDLP enzyme, the all-atoms force field of GROMOS 53a6 was used [30]. The parameters of GROMOS 53a6 were taken from the PRODRG [31]. The previous report on the protonation and deprotonation of several amino acids was adopted [32]. The simulation box was set to 8.8 × 8.8 × 8.8 nm, and the protein was solvated using around 20,000 SPC/E water model [33]. Finally, Na^+ ions were used to neutralize the charge of these systems.

In this study, the particle mesh Ewald method was used to rectify the 1.2 nm cut-off for the van der Waals energy terms and electrostatic interactions (PME) [34]. All bonds, including the H-containing bonds, were kept to fix using the LINCS algorithm [35]. Five hundred steps of steepest descent were performed for the initial minimization, followed by 100 ps equilibration. The equation of motion was integrated using the Leap-Frog algorithm [36]. The temperature and pressure of the HDLP-inhibitor system were tuned to 300 K and 1 bar using Berendsen's weak coupling algorithm [37]. The sampling step was run for 100 ns with a 0.002 ps, and the trajectories were stored every one ps period.

Quantum chemical viewing tools such as Rasmol [38], Pymol [27], and Chimera [22] were used in Linux and Windows operating systems. Finally, graphs were viewed and converted into PNG format using Grace Software.

Binding Energy Calculation

The g_energy from GROMACS was used to compute the average interaction energy. The total non-bonded potential energy (EP.E) and Coulombic short-range (CoulSR) potentials were used to compute the average interaction energy (I) between the enzyme and inhibitor.

$$EP.E = EP.E(repulsion) + EP.E(attraction) \quad (1)$$

$$EP.E = \frac{B}{r^{12}} - \frac{A}{r^{6}} \quad (2)$$

where A and B represent the Lennard-Jones parameters and r is the distance between inhibitor and enzyme. The Interaction energy (I) could be calculated using Eq. (4):

$$I = EP.E + CoulSR \quad (3)$$

$$I = 4\varepsilon\left[\left(\frac{\sigma}{r}\right)^{12} - \left(\frac{\sigma}{r}\right)^{6}\right] + \frac{e^2}{4\pi\varepsilon_0 r} \quad (4)$$

MM-PBSA was used to investigate the binding free energy between the HDLP enzyme and inhibitor. The binding free energy in MM-PBSA was specified as [39].

$$\Delta G_{binding} = \Delta G_{complex} - \left(\Delta G_{HDLP\ enzyme} + \Delta G_{inhibitor}\right) \quad (5)$$

The $\Delta G_{complex}$ is the total free energy of the complex. The $G_{HDLP\ enzyme}$ and $G_{inhibitor}$ are total free energies of enzymes and inhibitors, respectively.

Furthermore, Eq. (6) can be decomposed into its respective contributions [39].

$$\Delta G_{binding} = \Delta G_{MM} + \Delta G_{sol} - \Delta T_S \quad (6)$$

ΔG_{MM} and ΔG_{sol} can be written in the form of Eq. (7) and (8) [39].

$$\Delta G_{MM} = \Delta G_{int} + \Delta G_{elec} + \Delta G_{vdw} \quad (7)$$

$$\Delta G_{sol} = \Delta G_{PB} + \Delta G_{SA} \quad (8)$$

The internal energy, electrostatic energy, and van der Waals energy are denoted by the letters ΔG_{int}, ΔG_{elec}, and ΔG_{vdw}, respectively. The abbreviations ΔG_{PB} and ΔG_{SA} are used in Eq. (8) to describe the polar and nonpolar contributions between the solute and the continuum solvent [39].

Finally, the Gibbs free energy obtained from MM-PBSA can be written as Eq. (9):

$$\Delta G_{binding} = \left(\Delta G_{elec} + \Delta G_{vdw}\right) + \Delta G_{polar} + \Delta G_{nonpolar} \quad (9)$$

■ RESULTS AND DISCUSSION

The analysis of the obtained trajectories from MD simulations was done to investigate the stability of HDLP enzyme-inhibitor complexes. In this work, the

complex of HDLP-SAHA and the wild-type HDLP enzyme system were analyzed separately.

Toxicity Analysis

Drug design must take into account absorption, distribution, metabolism, excretion, and toxicity (ADME/Tox). Fortunately, in silico experiments can be used to anticipate these features. FAF-Drugs4 (Free ADME/Tox Filtering Tool), an online server, was used in this study to assess the ADMET/Tox properties of the medicinal compounds [40].

Lipinski's RO5 rule has been used in contemporary in silico toxicity studies to study toxicity. According to Lipinski's rule, the number of hydrogen bond donors must be no more than five, the number of hydrogen bond acceptors must not exceed ten, the molecular mass must not exceed 500 Daltons, and the log P (octanol-water partition coefficient) must be no more than five. A medication that becomes active when consumed orally can only break one of the rules.

Additionally, the toolbox for ADME/Tox filtering enables compound selection using ADME/Tox filtering rules such as molecular weight, logP, tPSA, number of rotating and rigid bonds, flexibility, HBD, HBA, H-bonds, total charge, solubility, and more.

The final status of all drug compounds is accepted after applying all ADME/Tox filtering rules. This finding indicates the values obtained from the FAF-Drug4 accessible server are agreed with the reference values of filters available in the FAF-Drug4.

Interaction Energy

In this study, the average interaction energies between the HDLP enzyme and its inhibitors were determined by adding the short- and long-range Lennard-Jones potentials to the corresponding Coulombic short-range potentials. The interaction energy between inhibitors and the HDLP enzyme is summarized in Table 3. The average interaction energies are arranged in the following order: CPD2 < SAHA < CPD3 < CPD1 < CPD4 < CPD5 < CPD6. The most stable complexes can be seen in CPD4, CPD5, and CPD6. These results suggest that HDLP-CPD4, HDLP-CPD5, HDLP-CPD6, and CPD2 complexes are longer-lasting in the aqueous medium than the HDLP-SAHA complex (reference).

Root Mean Square Deviation (RMSD)

The RMSD analysis measures the average changes in distance between the atoms in the proteins. The initial configuration of the HDLP enzyme was used for reference in the RMSD analysis in this work.

Table 2. In-silico toxicity parameters and values

Parameters	SAHA	CPD1	CPD2	CPD3	CPD4	CPD5	CPD6	Reference value
MW	264.32	163.17	164.16	152.15	433.5	394.4	399.48	≤ 500
log P	1.86	1.32	0.07	-0.04	2.42	1.04	2.06	−3 to 3
tPSA	78.43	49.33	62.22	65.12	107.45	92.44	115.30	≤ 180
Rot. bond	8	2	2	2	11	5	11	≤ 11
HBD	3	2	2	3	3	3	5	≤ 5
HBA	5	3	4	4	8	8	7	≤ 10
Solubility	66769.6	27997.4	60882.7	66953.6	67618.2	22651.2	20905.0	N/A
LRV	0	0	0	0	0	0	0	0
PRV	0	0	0	0	0	0	0	0
VRB	0	0	0	0	0	0	0	0
Final status	Accepted as a nontoxic compound							

MW-Molecular Weight, log P-logarithm of the partition coefficient between *n*-octanol and water, tPSA-topological polar surface area, Rot. Bond-Number of rotatable bonds, HBD-Hydrogen Bond Donor, HBA-Hydrogen Bond Acceptor, LRV- Lipinski's rule violation, PRV- Pfizer's rule violation, VRB- Veber's rule violation

Table 3. The employed components estimate the interaction energy between HDLP and inhibitors in kJ/mol. The uncertainty was obtained using the trajectories of 10 ns of the production step

Complex	L-JLR (kJ/mol)	L-JSR (kJ/mol)	CoulSR (kJ/mol)	Interaction energy (kJ/mol)
HDLP-SAHA	-30.64 ± 1.20	-84.07 ± 0.80	-3.08 ± 0.05	-117.78 ± 3.20
HDLP-CPD1	-29.65 ± 2.80	-70.02 ± 1.30	-1.73 ± 0.03	-101.40 ± 4.80
HDLP-CPD2	-34.41 ± 4.40	-104.21 ± 1.20	-2.04 ± 0.02	-140.66 ± 2.90
HDLP-CPD3	-16.78 ± 3.60	-96.97 ± 1.90	-1.69 ± 0.02	-115.44 ± 5.60
HDLP-CPD4	-120.89 ± 1.10	-195.55 ± 1.40	-3.58 ± 0.04	-320.02 ± 7.50
HDLP-CPD5	-50.51 ± 5.90	-153.99 ± 0.98	-3.62 ± 0.03	-208.12 ± 6.70
HDLP-CPD6	-39.49 ± 4.50	-155.27 ± 0.65	-3.61 ± 0.05	-198.37 ± 3.30

The simulation maintains the obtained RMSD of the HDLP enzyme in the complexes (Fig. 3). An essential alteration in the RMSD is seen as a result of the HDLP's intermolecular interaction with the co-factor and its surrounding amino acids, which causes significant conformational changes [17]. With SAHA, CPD4, CPD5, and CPD06, the RMSD of the HDLP enzyme has a relatively stable value of 0.3 nm. The trend for HDLP enzymes with CPD1, CPD2, and CPD3 is, nevertheless, somewhat upward. The average RMSD value of the wild-type HDLP enzyme is 0.36 nm. In the same way, the moderate RMSD of SAHA, CPD1, CPD2, CPD3, CPD4, CPD5, and CPD6 complexes are 0.30, 0.38, 0.35, 0.37, 0.32, 0.33, and 0.33 nm, respectively. Based on the RMSD analysis, it can be concluded that a stable interaction between HDLP enzymes and various inhibitors was formed during the simulation time of 10 ns.

The Radius of Gyration (Rg)

The conformational stability was assessed using the radius of gyration analysis. In the Rg analysis, if the protein folding is stable during the simulation, then the Rg value will be relatively small and vice versa [41]. Additionally, the Rg value in relation to the inhibitor complex also reflects how dense the inhibitor complex's structure is. The obtained Rg values in this work are

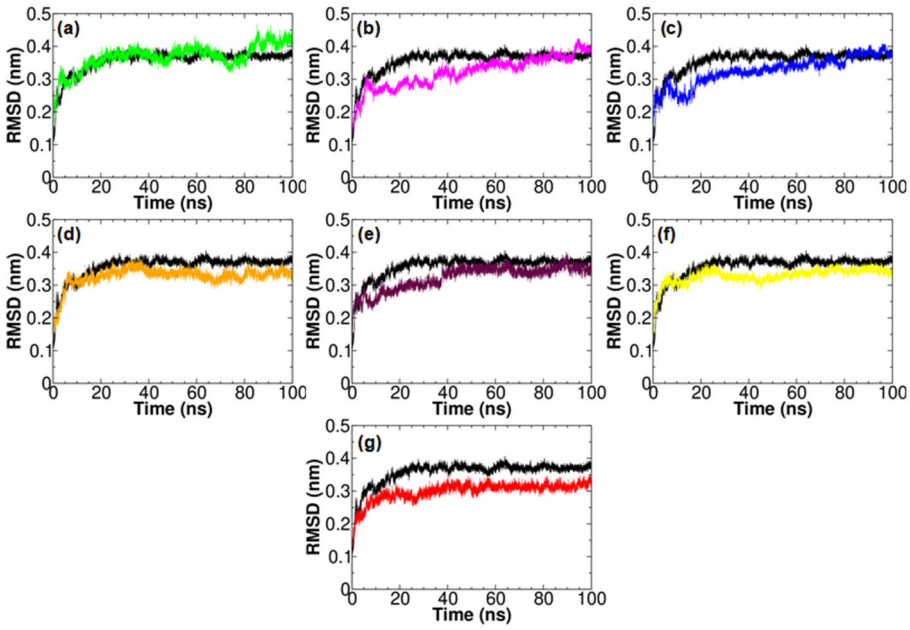

Fig 3. Backbone RMSD of (a) HDLP-CPD1, (b) HDLP-CPD2, (c) HDLP-CPD3, (d) HDLP-CPD4, (e) HDLP-CPD5, (f) HDLP-CPD6, and (g) HDLP- SAHA complexes (Black curve in (a) to (g) is the representation of the RMSD of the wild-type HDLP)

depicted in Fig. 4.

In this work, the obtained Rg values of SAHA, CPD1, CPD2, CPD3, CPD4, CPD5, and CPD6 are 1.94, 1.96, 1.95, and 1.95, 1.92, 1.94, and 1.94 nm, correspondingly. It can be inferred that the HDLP enzyme, after binding with SAHA, CPD1, CPD2, CPD4, CPD5, and CPD6, displays relatively similar behavior, and the compactness of the protein is maintained within reasonable stability. This statement is proved by the slight variation in the Rg values of 0.1 nm. In contrast, a slightly higher Rg value of 1.94 nm was observed in the wild-type HDLP enzyme.

Solvent-Accessible Surface Area (SASA)

SASA of proteins is one of the crucial things in the discussion of protein folding and stability analysis. Fig. 5 shows the acquired SASA of the enzyme in the HDLP-inhibitor complexes from our work.

All systems exhibited the same fluctuation trend until the 100 ns simulation time. The median SASA of wild-type HDLP enzyme is 87.67 nm^2. Likewise, the average SASA of SAHA, CPD1, CPD2, CPD3, CPD4, CPD5, and CPD6 complexes are 88.30, 85.0, 88.90, 85.92, 90.85, 89.68, and 89.38 nm^2, respectively. All the HDLP-inhibitor complexes show a relatively similar value for SASA, indicating the stable interaction between enzymes and complexes. The highest value is assigned to the HDLP-CPD4 complex.

Secondary Structure Analysis

The secondary structure of HDLP was investigated using the Stride website [42]. Fig. 6 shows the HDLP secondary structure.

The Stride web server also provides additional data, such as a numerical depiction of alpha-helical, beta-sheet, and other secondary structures, which is listed in Table 4.

The alpha-helical and beta-sheet secondary structures are the most prevalent, as shown in Table 4. It is more likely for hydrogen bond interactions to form in the alpha-helical structure than in the beta-pleated sheet's structure. Consequently, the folded alpha-helical structure is typically more resilient than the beta-sheet form. As a result, the HDLP structure with the highest alpha-helical content and the lowest beta-sheet content is the one that persists the longest. The HDLP enzyme contains greater alpha-helical and fewer beta-sheet structures than the wild-type HDLP enzyme, except for CPD3, according to assay data.

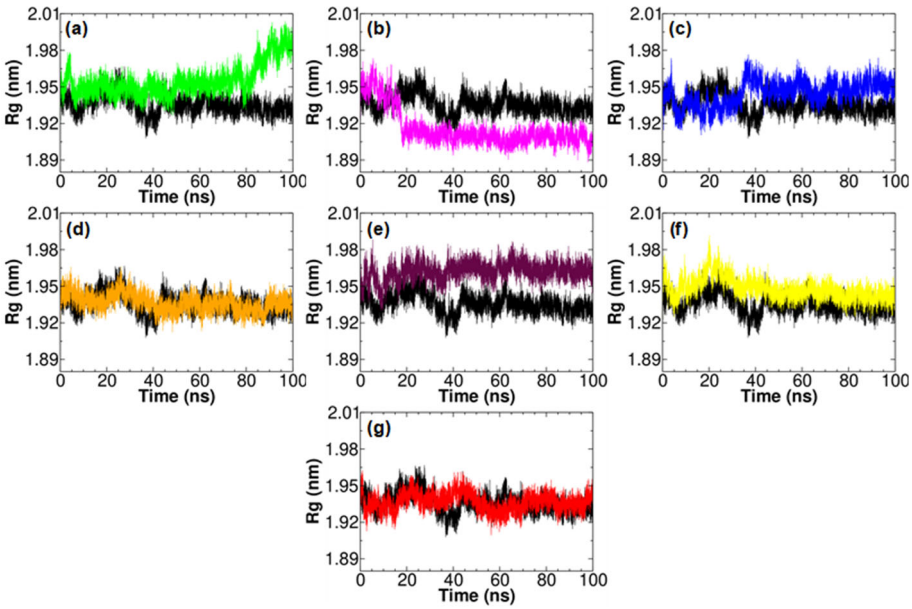

Fig 4. The Rg values of HDLP enzyme with (a) HDLP-CPD1, (b) HDLP-CPD2, (c) HDLP-CPD3, (d) HDLP-CPD4, (e) HDLP-CPD5, (f) HDLP-CPD6, and (g) HDLP- SAHA (Black curve in (a) to (g) shows the Rg of the wild type HDLP enzyme)

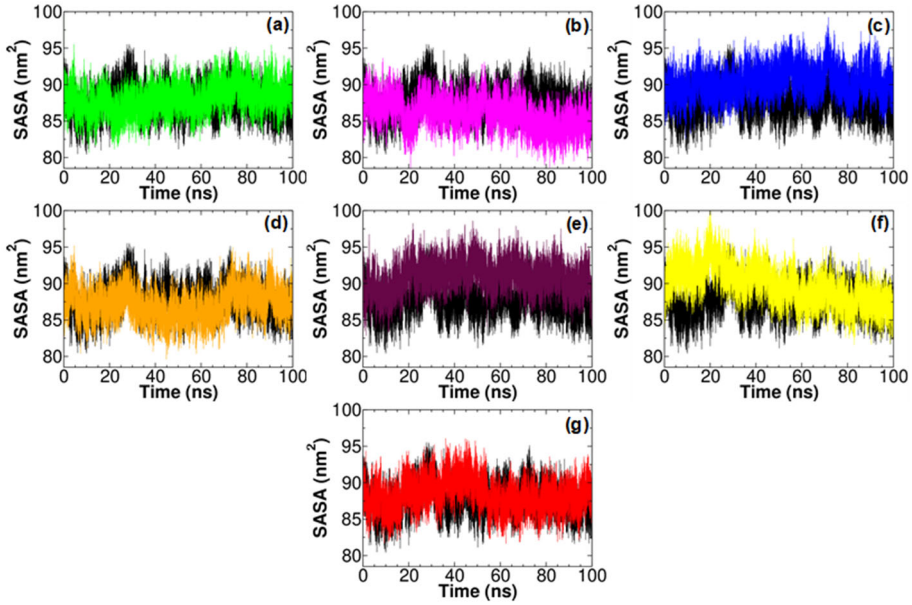

Fig 5. The SASA of HDLP-enzyme with (a) HDLP-CPD1, (b) HDLP-CPD2, (c) HDLP-CPD3, (d) HDLP-CPD4, (e) HDLP-CPD5, (f) HDLP-CPD6, and (g) HDLP- SAHA (Black curve in (a) to (g) represents the solvent accessible surface of the wild type HDLP)

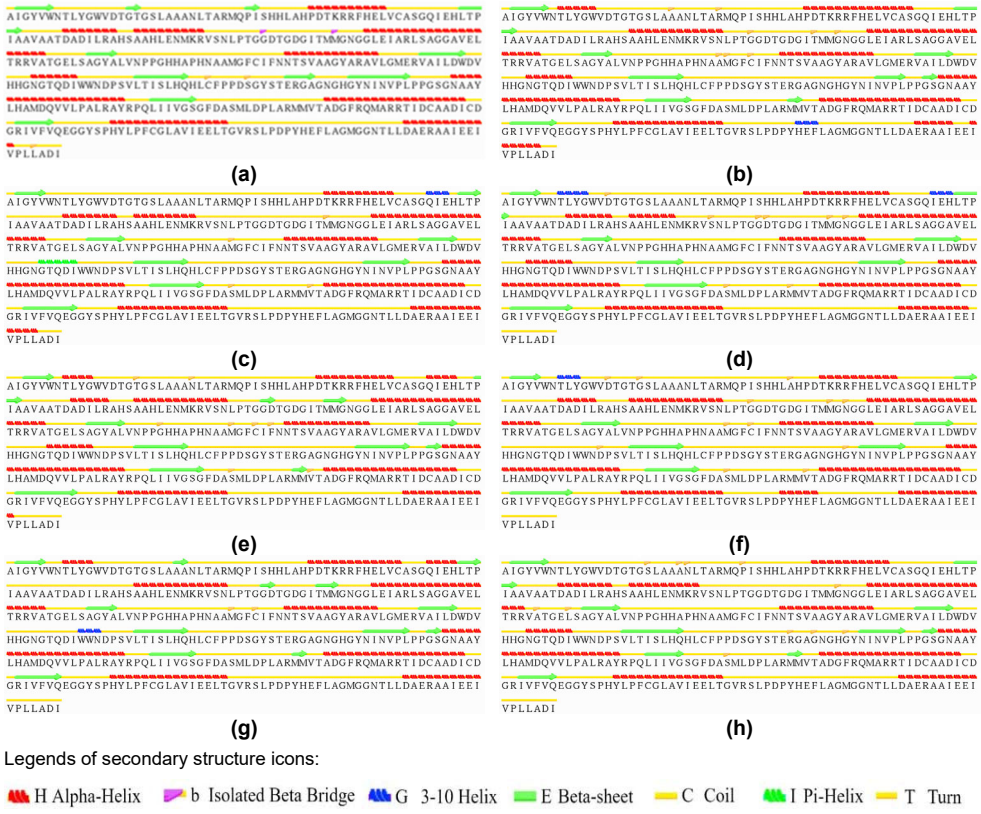

Fig 6. An illustration of the HDLP enzyme's secondary structure in (a) HDLP-CPD1, (b) HDLP-CPD2, (c) HDLP-CPD3, (d) HDLP-CPD4, (e) HDLP-CPD5, (f) HDLP-CPD6, (g) HDLP- SAHA, and (h) wild type HDLP enzyme

Table 4. Numerical representation of secondary structure information obtained from the stride web portal

HDLP-inhibitor complex	Alpha-Helical structure	Strand structure	Turn structure	Coil structure	Bridge structure	Pi-Helix structure	3,10 Helix structure
Wild	125	49	116	71	6	0	0
SAHA	126	52	100	84	2	0	3
CPD1	127	54	100	84	2	0	0
CPD2	131	46	105	74	8	0	0
CPD3	120	44	119	72	4	5	3
CPD4	126	46	111	73	8	0	0
CPD5	133	55	108	63	8	0	0
CPD6	127	45	102	86	12	0	3

Ramachandran Plot

The Ramachandran plot plots the dihedral angles of amino acid residues (ϕ and ψ) contained in a protein. Moreover, the plot is well-used to certify the conformation of amino acid residues and peptides in a protein. There are three crucial regions in the Ramachandran plot: the favored region (red color), the allowed region (yellow and faint yellow colors), and the banned zone (yellow and pale-yellow colors) (white color). The favored and allowed alpha-helical and beta-sheet structures occupy zones. According to the Ramachandran plot analysis, a high-quality model should have more than 90% of the amino acids in the preferred region [43]. The PROCHECK web portal was used to obtain the Ramachandran plots of the φ versus ψ angle of the HDLP enzyme and HDLP-inhibitor complexes [44]. Fig. 7 depicts the Ramachandran plot for the studied complexes.

Fig. 7 shows that most amino acid residues are located in favored and allowed regions according to their phi and psi angles, whereas very few residues are found in disallowed regions. On the other hand, a few of the wild-type HDLP enzyme's amino acid residues occur within the disallowed zone. Overall, in the HDLP enzyme with SAHA, CPD1, CPD2, CPD3, CPD4, CPD5, and CPD6 complexes, more than 90% of the amino acids are located in the most favored region (more than 90%), representing that all HDLP complexes show relatively more stable conformation after MD simulation.

Table 5 tells that generally, glycine residues lied in the disallowed region due to their hydrogen as a side chain, and the steric barrier within glycine is minimal.

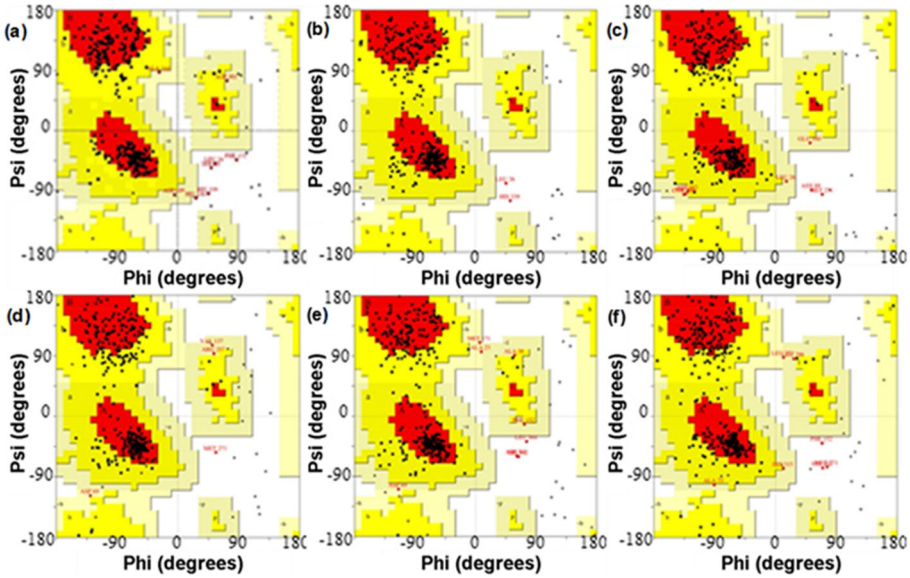

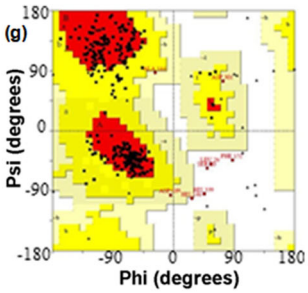

Fig 7. Ramachandran plot of phi and psi angle distributions of amino acids in (a) HDLP-CPD1, (b) HDLP-CPD2, (c) HDLP-CPD3, (d) HDLP-CPD4, (e) HDLP-CPD5, (f) HDLP-CPD6, (g) HDLP- SAHA

Therefore, the angles such as ϕ and ψ can rotate through a set of values. As a result, glycine deviates from the Ramachandran plot. Due to the cyclic side chain, the phi angle of the proline residue is similarly constrained. As a result, glycine and proline do not always adhere to the Ramachandran plot's stability criteria, and they end up in the forbidden territory.

Root-Mean-Square Fluctuation (RMSF)

RMSF method defines how much the amino acid residue in protein over time deviates from a reference position during simulation time in this study; the RMSF of each amino acid residue in the wild-type HDLP enzyme and HDLP-inhibitor complexes were calculated using the entire trajectories of 100 ns.

The flexibility of individual residues is reflected in the RMSF plot [45]. It can be inferred from Fig. 8 that the RMSF of all complexes are comparable, even though some amino acids exhibit a higher fluctuation. The residue in the bottom of HDLP's channel (His145, His146, His183, Gly154, Glu103, Gln254, Asp104, Tyr297, and Tyr308), in particular, shows the least amount of conformational changes among the amino acids in the active site. This finding suggests that in HDLP when the inhibitor is bound to the enzyme, some amino acids could shift significantly from their respective regular position. Still, binding with an inhibitor could make the amino acids in the enzyme's active site more rigid.

In the wild-type enzymes, the amino acid residues deviate an average of 0.120 nm, and the amino acids which have significant fluctuation with SAHA are CPD1, CPD2, CPD3, CPD4, CPD5, and CPD6 are 0.116, 0.131, 0.124, 0.128, 0.117, 0.119, and 0.122 nm, respectively.

Table 5. Plot statistics of HDLP-inhibitor complex obtained from Ramachandran plot

	SAHA	CPD1	CPD2	CPD3	CPD4	CPD5	CPD6
Residues in most favored regions	268 (88.2%)	269 (88.5%)	271 (89.1%)	274 (90.1%)	281 (92.4%)	278 (91.5%)	276 (90.8%)
Residues in additional allowed regions	30 (9.8%)	27 (8.9%)	31 (10.2%)	23 (7.6%)	19 (5.9%)	18 (5.9%)	21 (6.9%)
Residues in generously allowed regions	2 (0.7%)	4 (1.3%)	0 (0.0%)	5 (1.6%)	3 (1.0%)	5 (1.6%)	4 (1.3%)
Residues in disallowed regions	4 (1.3%)	4 (1.3%)	2 (0.7%)	2 (0.7%)	1 (0.3%)	3 (1.0%)	3 (1.0%)
Number of non-glycine and non-proline residues				304 (100.0%)			
Number of end-residues (excl. Gly and Pro)					4		
Number of glycine residues					40		
Number of proline residues					21		
Total number of residues					369		

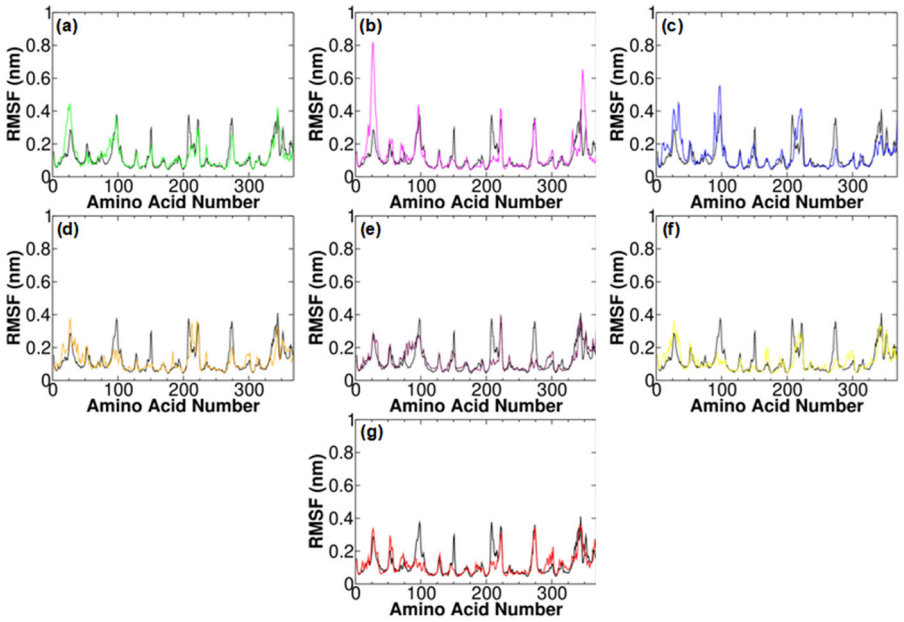

Fig 8. Amino acid RMSF in wild-type HDLP enzymes compared to (a) HDLP-CPD1, (b) HDLP-CPD2, (c) HDLP-CPD3, (d) HDLP-CPD4, (e) HDLP-CPD5, (f) HDLP-CPD6, and (g) HDLP- SAHA (For all figures, a black curve represents the RMSF of wild-type HDLP

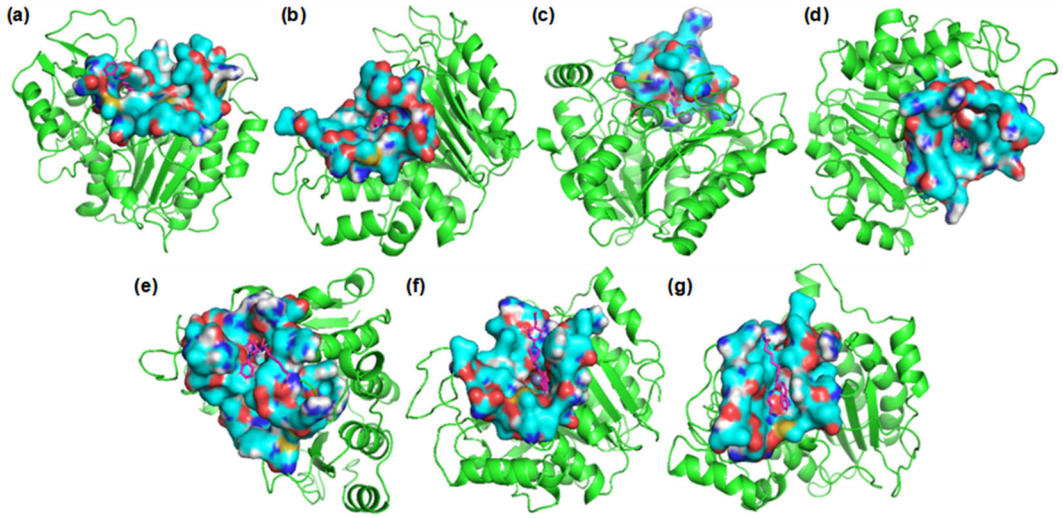

Fig 9. The inhibitor interacts with the amino acid in the cavity of HDLP. (a) HDLP-SAHA, (b) HDLP-CPD1, (c) HDLP-CPD2, (d) HDLP-CPD3, (e) HDLP-CPD4, (f) HDLP-CPD5, and (f) HDLP-CPD6 complexes

ARG29 residue in HDLP-CPD2 and HDLP-CPD3 complexes shows relatively high and similar fluctuation values, and other complexes show relatively low and almost identical fluctuation values. The higher RMSF with HDLP leads to weak binding affinity and generates less stable complexes. The smaller RMSF with HDLP leads to solid binding affinity and the generation of stable complexes.

Cavity Analysis of HDLP-Inhibitor Complex

The CavityPlus web service was used to identify the cavity in the HDLP enzyme [46]. On the surface of the HDLP enzyme structure, CavityPlus finds possible binding sites and rates them according to their drugability. The interaction of the inhibitor with the amino acids in the cavity area is shown in Fig. 9.

Some residues (47, 56, 52, and 50) are present in the cavity site of the HDLP enzyme complexes with SAHA, CPD4, CPD5, and CPD6. Fewer residues were found around CPD1 and CPD2, on the other hand. It makes sense that the interactions between the different inhibitors and the amino acid residues impact the number of holes in the HDLP that are accessible. There are more accessible cavities in HDLP in the wild-type (nine cavities) than in HDLP-inhibitor complexes. It is reasonable to predict that as proteins fold, the number of cavities will decrease. To discriminate between druggable and undruggable sections of the protein, use the cavity drug score value. The cavity with a high drug score will bind with the inhibitors. The cavity analysis's results are summarized in Table 6.

According to Table 6's findings, the HDLP cavities are reduced due to the inhibitor's interaction. The structure of the HDLP-inhibitor complex is typically compact. According to Table 6, CPD4, CPD5, and CPD6 have significant interactions with the cavity and high binding affinities, which leads to a stable complex. The interaction between the inhibitor and HDLP is weak in other complexes because they have low drug scores and binding affinities. In the SAHA, HDLP-CPD4, HDLP-CPD5, and HDLP-CPD6 complexes, more than 70% of the amino acids formed a druggable cavity. Like wild-type HDLP, more than 70% of the amino acids also formed the druggable cavity.

Zinc Geometry and Environment of the Active Site after Inhibitor Binding

With respect to the function of the inhibitors, the HDLP-inhibitor complexes' average druggable cavity volume varies. The wild-type HDLP has a volume of 140.950 $Å^3$, whereas the volume of HDLP-CPD1, HDLP-CPD2, HDLP-CPD3, HDLP-CPD4, HDLP-CPD5, HDLP-CPD6, and HDLP-SAHA complexes are, 180.05, 51.11, 175.98, 58.97, 80.33, 74.32, and 115.30 $Å^3$ respectively. The CASTp server was used to determine the cavities' volume. The findings showed that the cavity's amino acids flow toward the inhibitor when the inhibitor binds with it, creating a low-volume cavity. The compact and remarkably stable HDLP complex is shown by the low volume. As a result, it prevents other foreign substances from entering the cavity. However, the increment of the cavity volume in CPD1 and CPD3 could be linked to the low efficacy of CPD1 and CPD3. The results of the RMSD, Rg, Ramachandran plot, and secondary structure analyses are in agreement with this observation.

Table 6. Cavity results obtained from the CavityPlus web server

Complex	Cavity No.	Max. Pkd	Avg. Pkd	Drug score	Drugability
HDLP-SAHA	02	10.20	6.10	995.0	Strong
	01	10.56	6.18	298.0	Weak
HDLP-CPD1	02	9.69	5.94	-2.00	Medium
	01	10.49	6.21	-208.0	Weak
HDLP-CPD2	02	10.63	6.95	802.0	Strong
	01	11.21	6.43	126.0	Medium
	03	10.09	6.08	54.0	Medium
HDLP-CPD3	02	10.21	6.12	760.0	Strong
	01	10.44	6.20	13.0	Medium
	03	8.20	5.43	74.0	Medium
HDLP-CPD4	02	10.39	6.18	983.0	Strong
	01	10.64	6.27	291.0	Medium
HDLP-CPD5	01	11.90	6.76	933.0	Strong
	02	10.75	6.30	332.0	Medium
	03	9.46	5.86	24.0	Medium
HDLP-CPD6	01	9.90	6.01	864.0	Strong
	02	8.73	5.61	89.0	Medium

Numerous non-covalent interactions, including hydrogen bond interactions, electrostatic interactions, hydrophobic contacts, and van der Waals interactions, impact the stability of enzyme structures. The hydrophobic interactions operate as a driving force among these weak contacts, bringing the enzyme to a folded and stable form. The Zn(II) ion and the inhibitor's surroundings were examined using Ligplot+ [8].

According to the LigPlot+ data, the inhibitor and Zn(II) ion's immediate surroundings were heavily populated with water molecules at 0 nanoseconds. As a result, these solvent molecules will interact with the enzyme's active site amino acid residues. While some water molecules were dispersed, and some amino acids inhabited the area at 100 ns, on the other hand. Therefore, it is confirmed that interactions, including hydrophobic and hydrogen bonds, were produced during the MD simulation between the inhibitor and amino acid residues. These interactions increased the complex's stability and the enzyme's folded structure.

According to the Ramachandran plot analysis, Leucine 21 and Histidine 142 are present in the disallowed zone of the wild-type enzyme; however, these amino acids shifted to the allowed region when linked to CPD4, CPD5, and CPD6. The results of LigPlot+ are in Fig. 10, explaining the above observation. During the 100 ns MD simulation, Histidine 142 directly interacts with CPD4, CPD5, AND CPD6 through a hydrogen bond, and Leucine 21 interacts by hydrophobic interaction. Through these interactions, Leucine 21 and Histidine 142 become stable during MD simulation. Generally, based on Ramachandran plots, the proline residue will be observed in the Ramachandran plot's disallowed region. In contrast, Proline 32 will be observed in the allowed region due to its interaction with CPD1 through hydrophobic interactions.

Through the carbonyl and hydroxyl oxygens on the hydroxamic acid derivatives, Zn(II) ion coordinates to form a Penta-coordinated Zn (II). During the MD simulation, the shape and coordination number around the Zn(II) ion change. To explain the Zn(II) ion's observed coordination states, the coordination numbers were tracked throughout MD simulations. An octahedral geometry involving the two oxygen atoms of aspartic acid 268, two oxygen atoms of aspartic acid 180, one nitrogen atom of histidine 182, one carbonyl oxygen, and one hydroxyl oxygen of the inhibitor was produced in this study by the minimization and molecular dynamics of HDLP with CPD4. Contrarily, Zn(II) CPD2, CPD5, and CPD6 complexes reacted with the two oxygen atoms of aspartic acid 180, the two oxygen atoms of aspartic acid 268, and the one nitrogen atom of histidine 182.

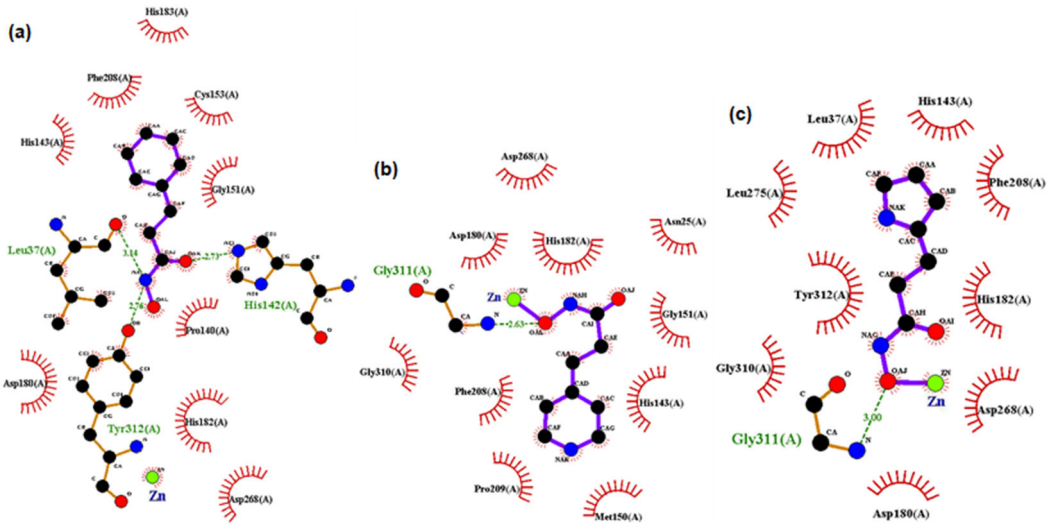

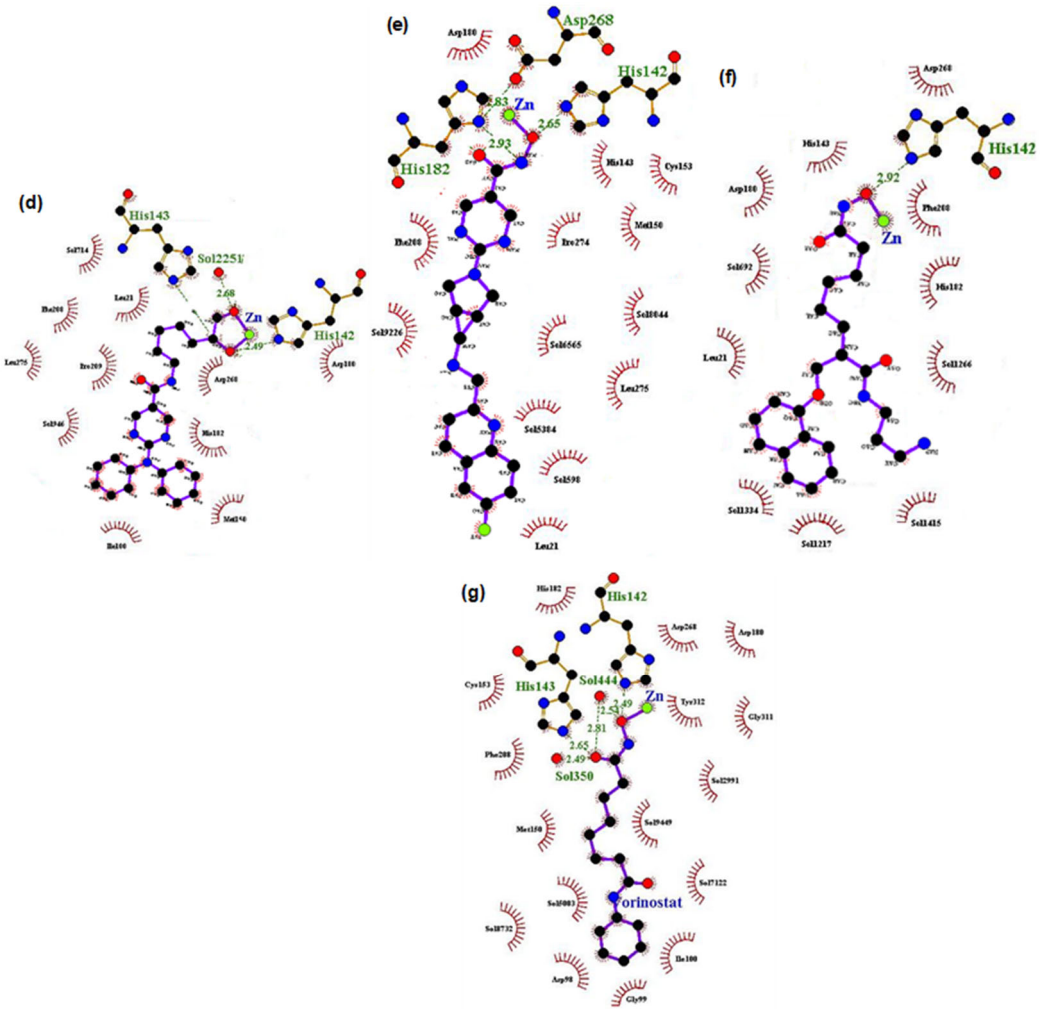

Fig 10. The inhibitor and Zinc co-factor in the HDLP enzyme and their environment. (a) CPD1, (b) CPD2, (c) CPD3, (d) CPD4, (e) CPD5, (f) CPD6, and (g) SAHA complexes

MM-PBSA Free Energy Analysis

The free binding energy word is the most appropriate one to use when discussing the binding affinities of protein-ligand complexes. The MM-PBSA method was used to calculate the binding free energies of the inhibitors to HDLP in order to analyze their binding affinity. The binding free energy was calculated using the g_mmpbsa. The calculation of the MM-PBSA binding free energy in the MM-PBSA framework included weak interactions such as Van der Waals energy, electrostatic energy, polar solvation energy, and SASA energy. The values of binding free energy are listed in Table 7.

The binding free energy for the HDLP-CPD4 complex was 475.33 kJ mol^{-1}, the most negative binding energy. The corresponding values are for the other complexes such as HDLP-CPD5, HDLP-CPD6, HDLP-CPD2, HDLP-CPD3, HDLP-SAHA, and HDLP-CPD1 -391.07, -362.80, -327.75, -321.53, -316.16, and -264.48 kJ mol^{-1}, respectively

Van der Waals and electrostatic interactions, which are weak intermolecular forces, aid in binding; nevertheless, polar solvation components contest the binding affinity. SASA also plays a role in stabilizing the binding. Conversely, the electrostatic interactions support the binding. The high stabilities of the HDLP-CPD4, HDLP-CPD5, and HDLP-CPD6 complexes were due to van der Waals, electrostatic, and SASA energies. In comparison to other HDLP-inhibitor complexes, those

Table 7. The calculated binding free energy and binding free energy components for seven inhibitors obtained from the MM-PBSA calculations

Complex	van der Waals energy (kJ/mol)	Electrostatic energy (kJ/mol)	Polar solvation energy (kJ/mol)	SASA energy (kJ/mol)	Binding free energy (kJ/mol)
HDLP-SAHA	75.03 ± 12.10	-826.25 ± 15.37	439.10 ± 5.73	-4.04 ± 0.72	-316.16 ± 7.78
HDLP-CPD1	77.02 ± 14.34	-839.51 ± 18.67	501.89 ± 5.04	-3.88 ± 0.67	-264.48 ± 9.57
HDLP-CPD2	88.82 ± 11.56	-885.81 ± 14.56	500.08 ± 8.78	-4.84 ± 0.94	-316.59 ± 6.23
HDLP-CPD3	85.51 ± 16.04	-890.95 ± 17.40	-498.29 ± 6.60	-4.38 ± 0.27	-311.53 ± 11.89
HDLP-CPD4	128.44 ± 13.38	-1058.92 ± 15.89	461.12 ± 11.59	-5.97 ± 0.35	-475.33 ± 14.92
HDLP-CPD5	97.75 ± 17.12	976.70 ± 11.30	492.53 ± 7.90	-4.65 ± 0.46	-391.07 ± 7.70
HDLP-CPD6	101.00 ± 16.08	-944.40 ± 12.68	485.76 ± 6.62	-5.10 ± 0.38	-362.80 ± 10.91

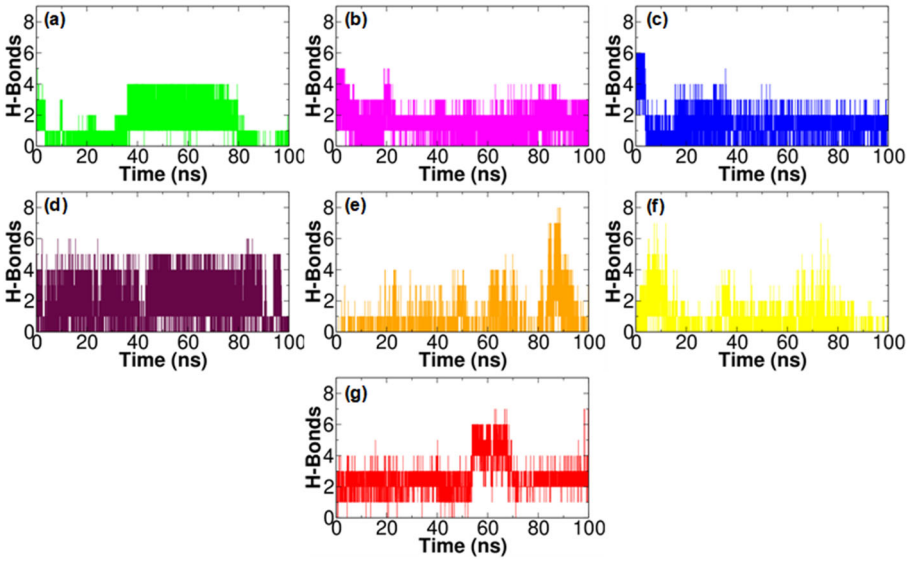

Fig 11. The formed intermolecular hydrogen bonds formed between active-site-residues of the HDLP with (a) SAHA, (b) CPD1, (c) CPD2, (d) CPD3, (e) CPD4, (f) CPD5, and (g) CPD6

containing CPD4, CPD5, and CPD6 showed higher electrostatic and binding energy values. CPD4, CPD5, and CPD6 also exhibited stronger binding stability to HDLP than the other inhibitors.

Hydrogen Bonds Analysis

The g_dist tool was used to look into the stability of hydrogen bonds. The hydrogen bonds that exist between the ligand and the protein have an impact on the stability of the complex [47]. Fig. 11 shows the number of hydrogen bonds between the HDLP and the medication molecules in each of the seven simulations.

The amino acid residues that interact with HDLP also be identified by investigating the formed hydrogen bonds between protein and ligand during the simulation time. The creation of hydrogen bonds between the ligand and the active site residues is another indicator of the ligand's propensity to bind to amino acid residues.

■ CONCLUSION

The inhibition feasibility of hydroxamic acid family inhibitors SAHA, CPD1, CPD2, CPD3, CPD4, CPD5, and CPD6 against the HDLP enzyme was investigated using MD simulation and trajectory analysis studies. The objective was achieved by examining the binding ability of inhibitors, structural changes of the HDLP enzyme due to inhibitor binding, stability of the HDLP-inhibitor complex's backbone, and positional stability of each amino acid. The stability of the HDLP enzyme and HDLP-inhibitor complexes in

the water systems is demonstrated by RMSD, Rg, SASA, hydrogen bond analysis, and secondary structure analysis. During the simulation, the RMSD and Rg of the HDLP enzyme in HDLP-SAHA, HDLP-CPD4, HDLP-CPD5, and HDLP-CPD6 were very small and steady. Then as well, when these inhibitors were used, the SASA of the HDLP enzyme was quite high. As a result, SAHA > CPD4 > CPD5 > CPD6 > CPD2 > CPD3 > CPD1 is the order in which the HDLP-inhibitor complexes are substantial. The stabilization pattern generated by the Ramachandran plot is similar to the obtained pattern above. According to the RMSF data, amino acid variations are modest in the complexes of SAHA, CPD4, CPD5, and CPD6, indicating that the inhibitor-HDLP enzyme interaction is rigid. The stability order, based on the MM-PBSA, is CPD4 > CPD5 > CPD6 > CPD2 >SAHA > CPD3 > CPD1. The stability order based on the total of long-range Lennard-Jones potential energy, short-range Lennard-Jones potential energy, and short-range Coulomb energy is CPD4 > CPD5 > CPD6 > CPD2 > SAHA > CPD3 > CPD1. Compared to the other inhibitors, all energy models suggested that CPD4, CPD5, and CPD6 bind to the HDLP enzyme substantially. The toxicity of all inhibitor compounds used in this investigation was investigated. According to the results of the Free ADME/Tox Filtering Tool, all substances are nontoxic. The present work shows that CPD2, CPD4, CPD5, and CPD6 can be identified as lead compounds to inhibit HDLP. The inhibitors have comparatively more potential than SAHA to inhibit the deacetylation of histone proteins. This provisional study will help estimate the feasibility of the novel HDAC inhibitors in cancer treatment.

■ ACKNOWLEDGMENTS

This research work is dedicated to the remembrance of the late Prof. (Mrs.) R. Maheswaran, an eminent scientist, chemist, academic, and science administrator in Sri Lanka, on the occasion of her death anniversary.

■ REFERENCES

[1] Jacobs, L.A., and Shulman, L.N., 2017, Follow-up care of cancer survivors: Challenges and solutions, *Lancet Oncol.*, 18 (1), e19–e29.

[2] Leeman, J.E., Romesser, P.B., Zhou, Y., McBride, S., Riaz, N., Sherman, E., Cohen, M.A., Cahlon, O., and Lee, N., 2017, Proton therapy for head and neck cancer: Expanding the therapeutic window, *Lancet Oncol.*, 18 (5), e254–e265.

[3] Eckschlager, T., Plch, J., Stiborova, M., and Hrabeta, J., 2017, Histone deacetylase inhibitors as anticancer drugs, *Int. J. Mol. Sci.*, 18 (7), 1414.

[4] Chrun, E.S., Modolo, F., and Daniel, F.I., 2017, Histone modifications: A review about the presence of this epigenetic phenomenon in carcinogenesis, *Pathol., Res. Pract.*, 213 (11), 1329–1339.

[5] Cavalieri, V., 2021, The expanding constellation of histone post-translational modifications in the epigenetic landscape, *Genes*, 12 (10), 1596.

[6] Dushanan, R., Weerasinghe, S., Dissanayake, D., and Senthilnithy, R., 2022, Driving the new generation histone deacetylase inhibitors in cancer therapy; Manipulation of the histone abbreviation at the epigenetic level: An in-silico approach, *Can. J. Chem.*, e-First.

[7] Dushanan, R., Weerasinghe, S., Dissanayake, D.P., and Senthilnithy, R., 2021, An in-silico approach to evaluate the inhibitory potency of selected hydroxamic acid derivatives on zinc-dependent histone deacetylase enzyme, *J. Comput. Biophys. Chem.*, 20 (6), 603–618.

[8] Dushanan, R., Weerasinghe, S., Dissanayake, D.P., and Senthilnithy, R., 2022, Cracking a cancer code histone deacetylation in epigenetic: The implication from molecular dynamics simulations on efficacy assessment of histone deacetylase inhibitors, *J. Biomol. Struct. Dyn.*, 40 (5), 2352–2368.

[9] Cappellacci, L., Perinelli, D.R., Maggi, F., Grifantini, M., and Petrelli, R., 2018, Recent progress in histone deacetylase inhibitors as anticancer agents, *Curr. Med. Chem.*, 27 (15), 2449–2493.

[10] Seto, E., and Yoshida, M., 2014, Erasers of histone acetylation: The histone deacetylase enzymes, *Cold Spring Harbor Perspect. Biol.*, 6 (4), a018713.

[11] Ganai, S.A., Shanmugam, K., and Mahadevan, V., 2015, Energy-optimised pharmacophore approach to identify potential hotspots during inhibition of

class II HDAC isoforms, *J. Biomol. Struct. Dyn.*, 33 (2), 374–387.

[12] Stiborová, M., Eckschlager, T., Poljaková, J., Hraběta, J., Adam, V., Kizek, R., and Frei, E., 2012, The synergistic effects of DNA-targeted chemotherapeutics and histone deacetylase inhibitors as therapeutic strategies for cancer treatment, *Curr. Med. Chem.*, 19 (25), 4218–4238.

[13] Ibrahim Uba, A., and Yelekçi, K., 2019, Homology modeling of human histone deacetylase 10 and design of potential selective inhibitors, *J. Biomol. Struct. Dyn.*, 37 (14), 3627–3636.

[14] Senthilnithy, R., Gunawardhana, H.D., De Costa, M.D.P., and Dissanayake, D.P., 2006, Absolute pK_a determination for *N*-phenylbenzohydroxamic acid derivatives, *J. Mol. Struct.: THEOCHEM*, 761 (1-3), 21–26.

[15] Senthilnithy, R., de Costa, M.D.P., and Gunawardhana, H.D., 2008, The pK_a values of ligands and stability constants of the complexes of Fe(III), Cu(II) and Ni(II) with some hydroxamic acids: A comparative study of three different potentiometric methods, *J. Natl. Sci. Found. Sri Lanka*, 36 (3), 191–198.

[16] Nielsen, T.K., Hildmann, C., Dickmanns, A., Schwienhorst, A., and Ficner, R., 2005, Crystal structure of a bacterial class 2 histone deacetylase homologue, *J. Mol. Biol.*, 354 (1), 107–120.

[17] Yan, C., Xiu, Z., Li, X., Li, S., Hao, C., and Teng, H., 2008, Comparative molecular dynamics simulations of histone deacetylase-like protein: Binding modes and free energy analysis to hydroxamic acid inhibitors, *Proteins: Struct., Funct., Bioinf.*, 73 (1), 134–149.

[18] Zhou, J., Xie, H., Liu, Z., Luo, H.B., and Wu, R., 2014, Structure-function analysis of the conserved tyrosine and diverse π-stacking among class I histone deacetylases: A QM (DFT)/MM MD study, *J. Chem. Inf. Model.*, 54 (11), 3162–3171.

[19] Trejo-Muñoz, C.R., Vázquez-Ramírez, R., Mendoza, L., and Kubli-Garfias, C., 2018, Biophysical mechanism of the SAHA inhibition of Zn^{2+}-histone deacetylase-like protein (FB188 HDAH) assessed via crystal structure analysis, *Comput. Mol. Biosci.*, 8 (2), 91–114.

[20] Lu, W., Zhang, R., Jiang, H., Zhang, H., and Luo, C., 2018, Computer-aided drug design in epigenetics, *Front. Chem.*, 6, 57.

[21] Kumari, R., Kumar, R., and Lynn, A., 2014, *g-mmpbsa*-A GROMACS tool for high-throughput MM-PBSA calculations, *J. Chem. Inf. Model.*, 54 (7), 1951–1962.

[22] Goddard, T.D., Huang, C.C., and Ferrin, T.E., 2005, Software extensions to UCSF Chimera for interactive visualization of large molecular assemblies, *Structure*, 13 (3), 473–482.

[23] Frisch, M.J., Trucks, G.W., Schlegel, H.B., Scuseria, G.E., Robb, M.A., Cheeseman, J.R., Scalmani, G., Barone, V., Mennucci, B., Petersson, G.A., Nakatsuji, H., Caricato, M., Li, X., Hratchian, H.P., Izmaylov, A.F., Bloino, J., Zheng, G., Sonnenberg, J.L., Hada, M., Ehara, M., Toyota, K., Fukuda, R., Hasegawa, J., Ishida, M., Nakajima, T., Honda, Y., Kitao, O., Nakai, H., Vreven, T., Montgomery, Jr., J.A., Peralta, J.E., Ogliaro, F., Bearpark, M., Heyd, J.J., Brothers, E., Kudin, K.N., Staroverov, V.N., Kobayashi, R., Normand, J., Raghavachari, K., Rendell, A., Burant, J.C., Iyengar, S.S., Tomasi, J., Cossi, M., Rega, N., Millam, J.M., Klene, M., Knox, J.E., Cross, J.B., Bakken, V., Adamo, C., Jaramillo, J., Gomperts, R., Stratmann, R.E., Yazyev, O., Austin, A.J., Cammi, R., Pomelli, C., Ochterski, J.W., Martin, R.L., Morokuma, K., Zakrzewski, V.G., Voth, G.A., Salvador, P., Dannenberg, J.J., Dapprich, S., Daniels, A.D., Farkas, O., Foresman, J.B., Ortiz, J.V., Cioslowski, J., and Fox, D.J., 2009, *Gaussian 09, Revision A.02*, Gaussian, Inc., Wallingford CT.

[24] Hanwell, M.D., Curtis, D.E., Lonie, D.C., Vandermeersch, T., Zurek, E., and Hutchison, G.R., 2012, Avogadro: An advanced semantic chemical editor, visualization, and analysis platform, *J. Cheminf.*, 4 (1), 17.

[25] Di Muzio, E., Toti, D., and Polticelli, F., 2017, DockingApp: A user friendly interface for

facilitated docking simulations with AutoDock Vina, *J. Comput.-Aided Mol. Des.*, 31 (2), 213–218.

[26] Therrien, E., Weill, N., Tomberg, A., Corbeil, C.R., Lee, D., and Moitessier, N., 2014, Docking ligands into flexible and solvated macromolecules. 7. Impact of protein flexibility and water molecules on docking-based virtual screening accuracy, *J. Chem. Inf. Model.*, 54 (11), 3198–3210.

[27] Yuan, S., Chan, H.C.S., and Hu, Z., 2017, Using PyMOL as a platform for computational drug design, *WIREs Comput. Mol. Sci.*, 7 (2), e1298.

[28] Raj, S., Sasidharan, S., Dubey, V.K., and Saudagar, P., 2019, Identification of lead molecules against potential drug target protein MAPK4 from *L. donovani*: An in-silico approach using docking, molecular dynamics and binding free energy calculation, *PLoS One*, 14 (8), e0221331.

[29] Pronk, S., Páll, S., Schulz, R., Larsson, P., Bjelkmar, P., Apostolov, R., Shirts, M.R., Smith, J.C., Kasson, P.M., van der Spoel, D., Hess, B., and Lindahl, E., 2013, GROMACS 4.5: A high-throughput and highly parallel open source molecular simulation toolkit, *Bioinformatics*, 29 (7), 845–854.

[30] Chen, P., Nishiyama, Y., and Mazeau, K., 2014, Atomic partial charges and one Lennard-Jones parameter crucial to model cellulose allomorphs, *Cellulose*, 21 (4), 2207–2217.

[31] Yousefpour, A., Amjad Iranagh, S., Nademi, Y., and Modarress, H., 2013, Molecular dynamics simulation of nonsteroidal antiinflammatory drugs, naproxen and relafen, in a lipid bilayer membrane, *Int. J. Quantum Chem.*, 113 (15), 1919–1930.

[32] Tummanapelli, A.K., and Vasudevan, S., 2015, Ab initio molecular dynamics simulations of amino acids in aqueous solutions: Estimating pK_a values from metadynamics sampling, *J. Phys. Chem. B*, 119 (37), 12249–12255.

[33] Prakash, M., Lemaire, T., Di Tommaso, D., de Leeuw, N., Lewerenz, M., Caruel, M., and Naili, S., 2017, Transport properties of water molecules confined between hydroxyapaptite surfaces: A Molecular dynamics simulation approach, *Appl. Surf. Sci.*, 418, 296–301.

[34] Huang, Y., Chen, W., Wallace, J.A., and Shen, J., 2016, All-atom continuous constant pH molecular dynamics with particle mesh ewald and titratable water, *J. Chem. Theory Comput.*, 12 (11), 5411–5421.

[35] Abraham, M.J., Murtola, T., Schulz, R., Páll, S., Smith, J.C., Hess, B., and Lindah, E., 2015, GROMACS: High performance molecular simulations through multi-level parallelism from laptops to supercomputers, *SoftwareX*, 1-2, 19–25.

[36] Anbarasu, K., and Jayanthi, S., 2018, Identification of curcumin derivatives as human $LMTK_3$ inhibitors for breast cancer: A docking, dynamics, and MM/PBSA approach, *3 Biotech*, 8 (5), 228.

[37] Serhan, M., Jackemeyer, D., Long, M., Sprowls, M., Diez Perez, I., Maret, W., Chen, F., Tao, N., and Forzani, E., 2020, Total iron measurement in human serum with a smartphone-based assay, *IEEE J. Transl. Eng. Health Med.*, 8, 1–9.

[38] Bernstein, H.J., 2000, Recent changes to RasMol, recombining the variants, *Trends Biochem. Sci.*, 25 (9), 453–455.

[39] Wang, E., Sun, H., Wang, J., Wang, Z., Liu, H., Zhang, J.Z.H., and Hou, T., 2019, End-point binding free energy calculation with MM/PBSA and MM/GBSA: Strategies and applications in drug design, *Chem. Rev.*, 119 (16), 9478–9508.

[40] Lagorce, D., Bouslama, L., Becot, J., Miteva, M.A., and Villoutreix, B.O., 2017, FAF-Drugs4: Free ADME-tox filtering computations for chemical biology and early stages drug discovery, *Bioinformatics*, 33 (22), 3658–3660.

[41] Paligaspe, P., Weerasinghe, S., Dissanayake, D.P., and Senthilnithy, R., 2021, Impact of Cd(II) on the stability of human uracil DNA glycosylase enzyme; An implication of molecular dynamics trajectories on stability analysis, *J. Biomol. Struct. Dyn.*, 0 (0), 1–8.

[42] Heinig, M., and Frishman, D., 2004, STRIDE: A web server for secondary structure assignment from known atomic coordinates of proteins, *Nucleic Acids Res.*, 32 (Suppl. 2), W500–W502.

[43] Fährrolfes, R., Bietz, S., Flachsenberg, F., Meyder, A., Nittinger, E., Otto, T., Volkamer, A., and Rarey,

M., 2017, Proteins*Plus*: A web portal for structure analysis of macromolecules, *Nucleic Acids Res.*, 45 (W1), W337–W343.

[44] Sowmya, H., 2019, A comparative study of homology modeling algorithms for NPTX2 structure prediction, *Res. J. Pharm. Technol.*, 12 (4), 1895–1900.

[45] Agoni, C., Ramharack, P., and Soliman, M.E.S., 2018, Co-inhibition as a strategic therapeutic approach to overcome rifampin resistance in tuberculosis therapy: Atomistic insights, *Future Med. Chem.*, 10 (14), 1665–1675.

[46] Paligaspe, P., Weerasinghe, S., Dissanayake, D.P., and Senthilnithy, R., 2021, Identify the effect of As(III) on the structural stability of monomeric PKM2 and its carcinogenicity: A molecular dynamics and QM/MM based approach, *J. Mol. Struct.*, 1235, 130257.

[47] Dushanan, R., Samantha, W., Dhammike, D., and Senthilnithy, R., 2022, Implication of Ab Initio, QM/MM, and molecular dynamics calculations on the prediction of the therapeutic potential of some selected HDAC inhibitors, *Mol. Simul.*, 48 (16), 1464–1475.